The Astrophysical Journal, 688:636–646, 2008 November 20
© 2008. The American Astronomical Society. All rights reserved. Printed in U.S.A.

MASS AND ORBIT DETERMINATION FROM TRANSIT TIMING VARIATIONS OF EXOPLANETS

David Nesvorný[1] and Alessandro Morbidelli[1,2]
Received 2008 June 20; accepted 2008 July 29

ABSTRACT

The timing variations of transits of an exoplanet provide means of detecting additional planets in the system. The short-period and resonant variations of the transit signal are probably the most diagnostic of the perturbing planet's mass and orbit. The method can be sensitive to small perturbing masses near the transiting planet and for orbits at mean motion resonances. It is not evident, however, how the mass and orbit of the perturbing planet can be determined from the observed variations of transit times. This is a difficult inverse problem. Direct *N*-body integrations are computationally too expensive to provide an adequate sampling of parameter space. Here we develop an alternative method based on analytic perturbation theory. We find that this new method is typically $\sim 10^4$ times faster than direct *N*-body integrations. The perturbation theory that we use here has an adequate precision to predict timing variations for most planetary orbits except those with very large eccentricities where the expansion of the disturbing function is divergent. By applying the perturbation method to the inverse problem we determine the number and precision of the measured transit times that are required for the unique and correct characterization of the perturbing planet. We find that the required precision is typically a small fraction ($\sim$15%–30%) of the full transit timing variation amplitude. Very high precision observations of transits will therefore be needed. We discuss the optimal observation strategy to characterize a planetary system from the transit timing variations. We find that the timing of secondary transits, if measured with adequate precision, can help to alleviate the problem with the degeneracy of solutions of the inverse problem.

Subject headings: celestial mechanics — planetary systems

1. INTRODUCTION

The goal of this paper is to describe a method that could be used to determine planetary masses and orbits for exoplanetary systems where at least one of the planets is transiting over the disk of its host star. To define the problem, we assume that the parameters of the transiting planet such as its mass, semimajor axis, and eccentricity are known from the radial velocity measurements, and that a second planet gravitationally perturbs the orbital motion of the transiting planet and produces observable short-period variation in the timing of individual transits (Agol et al. 2005; Holman & Murray 2005). We then investigate how the parameters of the perturbing planet, such as its mass and orbit, can be determined from the observed transit timing variations (TTVs).

This is a difficult (inverse) problem. The simplest approach would be to use direct *N*-body integrations of a large sample of planetary systems (Steffen & Agol 2005; Agol & Steffen 2007) in an attempt to directly fit the observed TTV signal. This method, however, is extremely CPU expensive due to the large number of unknown parameters. In the simplest case, where the transiting planet has a near-zero eccentricity and the orbits are assumed to be coplanar, the three basic parameters of the perturbing planet that one would like to know are its mass, semimajor axis, and eccentricity. In addition, the TTV signal also depends on the orbital phase of the perturbing planet (as defined by the longitude at given epoch) and its longitude of pericenter. Because the pericenter longitude of the perturbing planet may precess (e.g., due to presence of additional planets exterior to it), we must include in the list of unknown parameters not only its initial phase but also its precession frequency. Therefore, there are six unknown parameters in total in this case. If, for example, 50 values are needed to resolve each of the six dimensions of parameter space, more than 10^{10} planetary systems would need to be tracked in total.

To speed up this calculation we develop a new method that avoids the need for extensive orbital integrations. The method is based on perturbation theory (Hori 1966; Deprit 1969). We calculate the transit time at any given epoch as a sum over Fourier terms with amplitudes and phases that are explicit functions of the unknown parameters. Our tests demonstrate that this method is typically $\sim 10^4$ times faster than direct orbital integrations. It allows us to calculate 100 transit times for 10^{10} planetary systems in about a day of CPU time.

We describe the new method in § 2 and test its precision in § 3. In § 4, we simulate synthetic TTVs with precise *N*-body integrations and attempt to determine the mass and orbit of the perturbing planet from them by the least-squares fit. We discuss the uncertainty of the best-fit parameters as a function of the observed number of transits, observational time base, orbit, and mass of the perturbing planet. The code described here is available on request.

2. METHOD

The TTV signal is a series of transit times, $t(j)$, with $1 \leq j \leq N$, where N is the total number of observed transits. The orbit period of the transiting planet, P_1, can be estimated from this data by linear regression. When P_1 is extracted from $t(j)$, we end up with variation $\delta t(j) = t(j) - jP_1$ that describes the difference of $t(j)$ from a strictly periodic (i.e., single-frequency) signal. This variation can be produced by additional planets in the system that gravitationally perturb the orbit of the transiting planet and advance or delay individual transits.

The dynamics of interacting planets can be complex. Probably the most diagnostic signatures for the TTV method are the short-period and (near-) resonant oscillations of the transiting planet's orbit produced by gravitational perturbations from other planets

[1] Department of Space Studies, Southwest Research Institute, 1050 Walnut Street., Suite 400, Boulder, CO 80302.
[2] Observatoire de la Côte d'Azur, Boulevard de l'Observatoire, BP 4229, 06304 Nice Cedex 4, France.

(Holman & Murray 2005; Agol et al. 2005).[3] Due to these perturbations, the true longitude of the transiting planet, θ_1, can slightly lead or trail the one of the unperturbed Keplerian orbit at the time of transit, therefore producing the timing variation. For an elliptic orbit, θ_1 can be written as a function of the mean longitude, λ_1, as

$$\theta_1 = \lambda_1 + \sum_{k=1}^{\infty} H_k(e_1) \sin k(\lambda_1 - \varpi_1), \tag{1}$$

where e_1 and ϖ_1 are the eccentricity and pericenter longitude of the transiting planet, and $H_k(e_1)$ are polynomials in e_1 with the lowest power of H_k in e_1 being k. Therefore, the TTV signal may arise from changes in λ_1, e_1, or ϖ_1. In practice, the eccentricity of transiting planets is typically small (Torres et al. 2008) because orbits have been circularized by tidal effects. To the lowest order in e_1, equation (1) becomes

$$\theta_1 = \lambda_1 + 2e_1 \sin(\lambda_1 - \varpi_1) + \mathcal{O}(e_1^2). \tag{2}$$

In regularized variables, $h_1 = e_1 \sin \varpi_1$ and $k_1 = e_1 \cos \varpi_1$; this leads to

$$n_1 \delta t = \delta\lambda_1 + 2\delta k_1 \sin(\lambda_1) - 2\delta h_1 \cos(\lambda_1) + \mathcal{O}(e_1), \tag{3}$$

where n_1 is the mean motion of the transiting planet, and $\delta\lambda_1$, δk_1, and δh_1 denote the short-period variations of the osculating orbital elements. For simplicity, we do not explicitly list terms $\mathcal{O}(e_1)$ in the above equation. These and higher order terms can be easily taken into account if e_1 is significant.

In the following, we will assume that $m_1, m_2 \ll m_0$, where m_0, m_1, and m_2 are masses of the star, inner (transiting), and outer planets, respectively, and determine the short-period variations in $\delta\lambda_1$, δh_1, and δk_1 using the perturbation theory. The Hamiltonian H of the two planets orbiting a central star is

$$H = H_0 + H_1, \tag{4}$$

where

$$H_0 = -\frac{Gm_0m_1}{2a_1} - \frac{Gm_0m_1}{2a_2} \tag{5}$$

and

$$H_1 = -Gm_1m_2\left[\frac{1}{|\boldsymbol{r}_1 - \boldsymbol{r}_2|} - \frac{\boldsymbol{r}_1 \cdot \boldsymbol{r}_2}{r_2^3}\right], \tag{6}$$

where G is the gravitational constant, $\boldsymbol{r}_1$ and $\boldsymbol{r}_2$ are the Jacobi coordinates of planets, and a_1 and a_2 are their semimajor axes (e.g., Brouwer & Clemence 1961).

We use the expansion of H_1 in the Fourier series:

$$H_1 = -\frac{Gm_1m_2}{a_2} \sum C_{\boldsymbol{k}}^{\boldsymbol{l},\boldsymbol{j}}(\alpha) e_1^{l_1} e_2^{l_2} \left(\sin\frac{i_1}{2}\right)^{j_1} \left(\sin\frac{i_2}{2}\right)^{j_2} \times \exp \iota(k_1\lambda_1 + k_2\lambda_2 + k_3\varpi_1 + k_4\varpi_2 + k_5\Omega_1 + k_6\Omega_2) \tag{7}$$

with $\iota = \sqrt{-1}$, $C_{\boldsymbol{k}}^{\boldsymbol{l},\boldsymbol{j}}(\alpha) = C_{-\boldsymbol{k}}^{\boldsymbol{l},\boldsymbol{j}}(\alpha)$, $\alpha = a_1/a_2 < 1$, and multi-indexes $\boldsymbol{l} = (l_1, l_2)$, $\boldsymbol{j} = (j_1, j_2)$, and $\boldsymbol{k} = (k_1, k_2, k_3, k_4, k_5, k_6)$. Properties of equation (6) imply that $\sum_{n=1}^{6} k_n = 0$, and that $j_1 + j_2$, $l_1 - |k_3|$, $l_2 - |k_4|$, $j_1 - |k_5|$, and $j_2 - |k_6|$ are even integers. The lowest combined power of eccentricities and inclinations that appears in front of each Fourier term in equation (7) is thus $l_1 + l_2 + j_1 + j_2 = \sum_{n=3}^{6} |k_n| \geq 0$ (see, e.g., Morbidelli 2002, pp. 35–36).

It is convenient to write equations (5) and (6) in terms of canonical Poincaré variables:

$$\begin{aligned} L_j &= m_j\sqrt{Gm_0a_j}, \quad \lambda_j \\ y_j &= \sqrt{2P_j}\cos p_j, \quad x_j = \sqrt{2P_j}\sin p_j \\ z_j &= \sqrt{2Q_j}\cos q_j, \quad v_j = \sqrt{2Q_j}\sin q_j, \end{aligned} \tag{8}$$

where

$$\begin{aligned} P_j &= L_j\left(1 - \sqrt{1 - e_j^2}\right), \quad p_j = -\varpi_j \\ Q_j &= L_j\sqrt{1 - e_j^2}(1 - \cos i_j), \quad q_j = -\Omega_j. \end{aligned} \tag{9}$$

The indexes $j = 1$ and $j = 2$ denote the variables of the inner and outer planets, respectively, and i_j and Ω_j are their inclinations and nodal longitudes. By substituting the Poincaré variables in equation (4) we find that

$$H = H_0(L_1, L_2) + H_1(L_j, y_j, z_j, \lambda_j, x_j, v_j) \tag{10}$$

with $H_1 \ll H_0$ for $m_1, m_2 \ll m_0$. We do not list the expressions for H_0 and H_1 in the Poincaré variables here. In fact, it is not necessary to calculate these expressions explicitly because our computer algebra code can easily deal with the transformation between the orbital elements and Poincaré variables, and thus combine equations (5)–(9) to obtain equation (10).

The perturbation theory (Hori 1966; Deprit 1969) allows us to select a canonical transformation from E_j to $\bar{E}_j$, where E denotes arbitrary Poincaré variable, that transforms H to the new Hamiltonian, $\bar{H}$, that does not depend on new coordinates $\bar{\lambda}_j$. The new momenta, $\bar{L}_j$, become constants of motion and $\bar{\lambda}_j = n_j t + \lambda_j^{(0)}$, where constants n_j and $\lambda_j^{(0)}$ denote the mean orbital frequency of planet j and initial phase angle, respectively.

The transformation between E_j and $\bar{E}_j$ can be given in terms of generating function χ as

$$E_j = \bar{E}_j + \sum_{n=1}^{\infty} \frac{1}{n!} \mathcal{L}_\chi^n \bar{E}_j, \tag{11}$$

where $\mathcal{L}_\chi^n$ is the Lie derivative defined in terms of Poisson brackets as

$$\begin{aligned} \mathcal{L}_\chi^1 \bar{E}_j &= \{\bar{E}_j, \chi\}, \\ \mathcal{L}_\chi^n \bar{E}_j &= \mathcal{L}_\chi^1 \mathcal{L}_\chi^{n-1} \bar{E}_j. \end{aligned} \tag{12}$$

Therefore, to the first order in m_2/m_0, the terms of equation (11) relevant to equation (3) are

$$\begin{aligned} \lambda_1 &= \bar{\lambda}_1 + \frac{\partial\chi_1}{\partial\bar{L}_1}, \\ x_1 &= \bar{x}_1 + \frac{\partial\chi_1}{\partial\bar{y}_1}, \\ y_1 &= \bar{y}_1 - \frac{\partial\chi_1}{\partial\bar{x}_1}, \end{aligned} \tag{13}$$

[3] The long-term effects such as the apsidal precession produced by the perturbing planet are more difficult to detect via TTVs if transit observations span only a few years (Heyl & Gladman 2007). In addition, these effects can be masked by contributions to the apsidal precession from the oblateness of the central star, relativity, and tides.

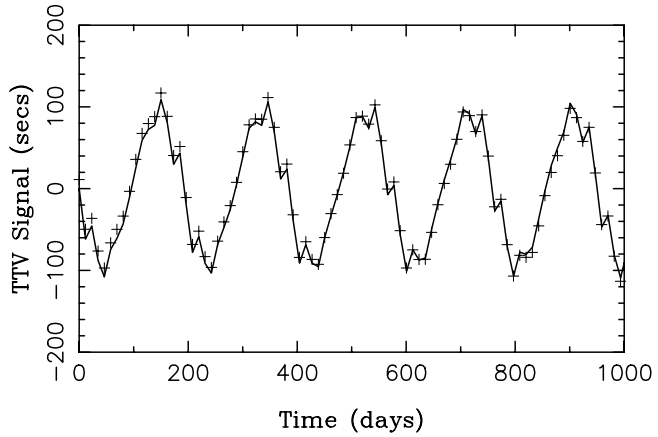

FIG. 1.—Comparison between the TTV signal determined from a precise numerical integration (*plus signs*) and the one obtained from the PT method (*solid line*). The transiting planet has $a_1 = 0.1$ AU and $e_1 = 0$. The perturbing planet has $m_2 = 10^{-4} m_0$, $a_2 = 0.2$ AU, and $e_2 = 0.1$. The precision of the perturbation theory is good in this case. The amplitude and QPT of the TTV signal are 234 s and 2.6% (see main text for the definition of QPT).

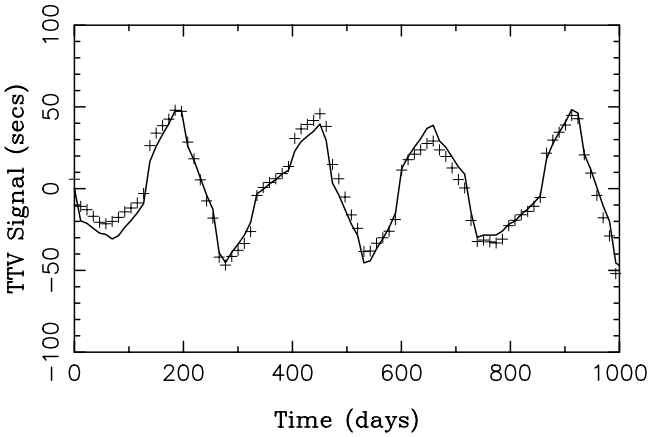

FIG. 2.—Same as Fig. 1, but for $a_2 = 0.32$ AU and $e_2 = 0.35$. This case tests the precision of the perturbation theory for a large orbital eccentricity of the perturbing planet. The amplitude and QPT of the TTV signal are 104 s and 5.4%.

where χ_1 denotes the first-order (linear) terms of χ in m_2/m_0. Explicit relations between $\delta k_1, \delta h_1$ and $\delta x_1 = x_1 - \bar{x}_1, \delta y_1 = y_1 - \bar{y}_1$ can be given from the definition of these variables. With H_1 defined in equation (7), χ_1 can be written as

$$\chi_1 = \frac{G m_1 m_2}{\bar{a}_2} \sum_{|k_1|+|k_2|\neq 0} \iota \frac{C_{\boldsymbol{k}}^{l,j}(\bar{\alpha})}{k_1 n_1 + k_2 n_2} \bar{e}_1^{l_1} \bar{e}_2^{l_2} \left(\sin\frac{\bar{i}_1}{2}\right)^{j_1} \times \left(\sin\frac{\bar{i}_2}{2}\right)^{j_2} \exp \iota\left(k_3 \bar{\varpi}_1 + k_4 \bar{\varpi}_2 + k_5 \bar{\Omega}_1 + k_6 \bar{\Omega}_2\right) \times \exp \iota\left(k_1 \bar{\lambda}_1 + k_2 \bar{\lambda}_2\right), \quad (14)$$

where $\bar{a}_2, \bar{\alpha} = \bar{a}_1/\bar{a}_2, \bar{e}_j, \bar{i}_j, \bar{\varpi}_j, \bar{\Omega}_j, \bar{\lambda}_j$ are functions of the new (mean) canonical momenta and coordinates.

Series in equation (14) is not convergent for $k_1 n_1 + k_2 n_2 \approx 0$, i.e., near mean motion resonances between the two planets. To deal with this complication we eliminate all Fourier terms from equation (14) with $k_1 n_1 + k_2 n_2 < n_2 f_{\rm cut}$, where $f_{\rm cut}$ is the cutoff parameter. Different values of $f_{\rm cut}$ are tested in § 3.

According to equation (13), we must take the derivative of χ_1 with respect to L_1, x_1, and y_1. For example, we have for $e_1 = i_1 = 0$ that

$$\frac{\partial \chi_1}{\partial \bar{L}_1} = \frac{\partial \bar{a}_1}{\partial \bar{L}_1} \frac{\partial \chi_1}{\partial \bar{a}_1} \quad (15)$$

with

$$\frac{\partial \bar{a}_1}{\partial \bar{L}_1} = \frac{2\sqrt{\bar{a}_1}}{m_1 \sqrt{G m_0}}. \quad (16)$$

Generating function χ_1 depends on $\bar{a}_1$ via $C_{\boldsymbol{k}}^{l,j}(\bar{a}_1/\bar{a}_2)$ and n_1. The corresponding derivative term is

$$\frac{\partial}{\partial \bar{a}_1}\left[\frac{C_{\boldsymbol{k}}^{l,j}(\bar{\alpha})}{k_1 n_1 + k_2 n_2}\right] = \frac{1}{k_1 n_1 + k_2 n_2}\left(\frac{\partial C_{\boldsymbol{k}}^{l,j}}{\partial \bar{a}_1} - \frac{k_1 C_{\boldsymbol{k}}^{l,j}}{k_1 n_1 + k_2 n_2} \frac{\partial n_1}{\partial \bar{a}_1}\right) \quad (17)$$

with

$$\frac{\partial n_1}{\partial \bar{a}_1} = -\frac{3}{2} \frac{\sqrt{G m_0}}{\bar{a}_1^{5/2}}. \quad (18)$$

The derivatives of χ_1 with respect to x_1 and y_1 can also be explicitly given. We do not list them here.

There are two alternative expressions for coefficients $C_{\boldsymbol{k}}^{l,j}$ that we can use: (1) in terms of Laplace coefficients $b_{s/2}^{(i)}(\alpha)$ (e.g., Ellis & Murray 2000); (2) in power series of α (e.g., Kaula 1962). These expressions are equivalent as Laplace coefficients can be expanded in power series of α. The domain of convergence of these series is given by the Sundman criterion (Sundman 1916), which postulates that the series is absolutely convergent for

$$a_2 g(e_1) > a_1 f(e_2), \quad (19)$$

where

$$g(e_1) = \sqrt{1 + e_1^2} \cosh w + e_1 + \sinh w, \quad (20)$$

$$f(e_2) = \sqrt{1 + e_2^2} \cosh z - e_2 - \sinh z \quad (21)$$

with $w = e_1 \cosh w$ and $z = e_2 \cosh z$. For example, for $\alpha = 0.5$ and $e_1 = 0$ the expansion is convergent for $e_2 < 0.32$. This limits the applicability of our method. We discuss this issue in more detail in § 3.

3. TESTS

The perturbation theory method (hereafter the PT method) described in the previous section has been implemented in C and Fortran computer codes. The C-language code (Šidlichovský 1990) was used to calculate a table of coefficients $C_{\boldsymbol{k}}^{l,j}$ (and their derivatives with respect to α) for 8000 values of α between 0.1 and 0.9. The code efficiently evaluates the power expansion of $C_{\boldsymbol{k}}^{l,j}$ in α (Kaula 1962) with the maximum power selected in such a way that the numerical values of $C_{\boldsymbol{k}}^{l,j}$ are precise to at least seven decimal digits. For $\alpha \sim 0.9$, this required accounting for powers up to ~300. To assure that the PT method is valid for moderate to large values of e_2, we used terms $e_2^{l_2}$ in equation (7) up to $l_2 = 15$. We verified that increasing the truncation order does not significantly improve the results. Our Fortran code reads the table of coefficients $C_{\boldsymbol{k}}^{l,j}$ (and $dC_{\boldsymbol{k}}^{l,j}/d\alpha$) and determines δt (eq. [3]) according to the PT method described in § 2. While our codes are capable of dealing with the case of nonzero inclinations, here we only discuss

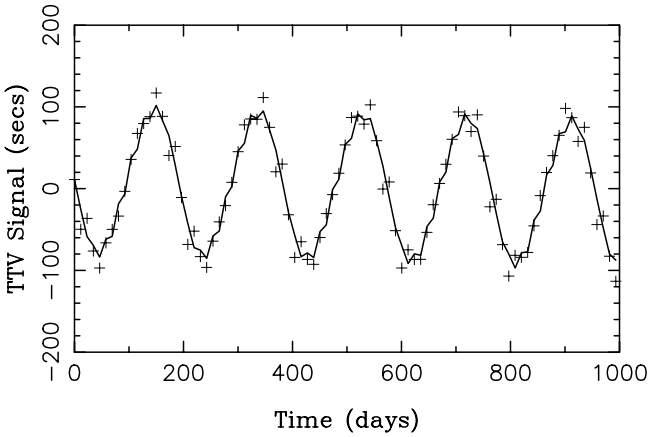

FIG. 10.— Example of the non-uniqueness of the inverse problem. Plus signs show the original TTV signal for our case-1 planetary system ($a_1 = 0.1$ AU, $e_1 = 0$, $m_2 = 10^{-4} m_0$, $a_2 = 0.2$ AU, and $e_2 = 0.1$). The solid line shows the TTV signal obtained with $m_2 = 1.4125 \times 10^{-4} m_0$, $a_2 = 0.15265$ AU, and $e_2 = 0.03$. This later solution was identified by the PT method as a fit to the original TTV data with $\eta = 15.6$ s. The two series of TTVs shown here would therefore be indistinguishable if the uncertainty of the TTV measurements exceeded ≈15 s.

4.1. *Three-parameter Fits*

We start by discussing the results based on equation (22). Figure 9 shows the best-fit solutions for case 1 ($m_2 = 10^{-4} m_0$, $a_2 = 0.2$ AU, and $e_2 = 0.1$). With $\eta_{\rm cut} = 10$ s, the least-squares fit identifies the correct mass and orbit of the outer planet with no significant ambiguity.

The uncertainty of determined parameters m_2 and e_2 significantly increases with increasing $\eta_{\rm cut}$. For example, these parameters are constrained only within $0.04 < e_2 < 0.25$ and $2 \times 10^{-5} < m_2/m_0 < 2.5 \times 10^{-4}$ for $\eta_{\rm cut} = 30$ s. In contrast, a_2 could be determined with an exquisite precision even for $\eta_{\rm cut} = 30$ s (Fig. 9). This result stems from the sensitivity of n_2 to the exact value of a_2 and its effects on the behavior of λ_2 in the argument of equation (14). For $\eta_{\rm cut} > 15$ s, however, additional (incorrect) solutions start to appear as acceptable fits, such as $m_2 \approx 1.5 \times 10^{-5} m_0$, $a_2 \approx 0.153$ AU, and $e_2 \lesssim 0.05$ (Fig. 10). Apparently, the inverse problem becomes non-unique for low signal-to-noise ratio (S/N). In particular, the noise can mask TTV harmonics that were crucial for the solution's uniqueness. With $\eta_{\rm cut} > 15$ s (in this case), only a few main harmonics can be resolved in TTVs. If that is the case the planet detection can still be achieved by the TTV method, but the characterization of the perturbing planet's parameters becomes ambiguous.

Interestingly, the critical level of $\eta_{\rm cut}$ that can ensure a unique (and correct) solution is rather a weak function of the number of transits that we include in our computation. For example, if we decrease the number of transits from the original 87 (corresponding to the continuous 1000 day transit data) to 22 (corresponding to 250 days), the uniqueness threshold does not change much and, in the specific case discussed here, remains at the ≈15 s level. Figure 11 shows the range of the best-fit orbital parameters for 43 and 22 transits. With only 10 transits (corresponding to 120 days), however, the inverse problem becomes ambiguous even for unrealistically small $\eta_{\rm cut}$ of order of a few seconds. We emphasize that these results were obtained with the three-parameter fit. Fits to a larger number of parameters would probably suffer from more ambiguity.

The best-fit solutions from 87 transits of the case-2 planetary system ($m_2 = 10^{-4} m_0$, $a_2 = 0.32$ AU, and $e_2 = 0.35$) and $\eta_{\rm cut} = 10$ s have $4 \times 10^{-5} < m_2/m_0 < 3 \times 10^{-4}$, $0.3198 < a_2 < 0.3201$ AU, and $0.26 < e < 0.42$. This is comfortably close to the original parameters. Incorrect solutions start to appear for $\eta_{\rm cut} > 10$ s.

Figure 12 shows the best-fit solutions for case 3 ($m_2 = 10^{-4} m_0$, $a_2 = 0.15$ AU, and $e_2 = 0.05$) and $\eta_{\rm cut} = 100$ s. They nicely match the input parameters. The uncertainty improves when we adopt lower levels of $\eta_{\rm cut}$. For example, $9 \times 10^{-5} < m_2/m_0 < 1.2 \times 10^{-4}$, $0.1499 < a_2 < 0.1501$ AU, and $0.03 < e < 0.08$ with $\eta_{\rm cut} = 50$ s. Ambiguous solutions arise for $\eta_{\rm cut} > 100$ s in this example. Therefore, the threshold value of $\eta_{\rm cut}$ in case 3 is about 1 mag larger than those in cases 1 and 2. We conclude that the compact planetary orbits (such as our case 3) can be more easily characterized from TTVs

The resonant case shown in Figure 7 ($m_2 = 10^{-4} m_0$, $a_2 = 0.25$ AU, and $e_2 = 0.2$) would be more difficult to identify with

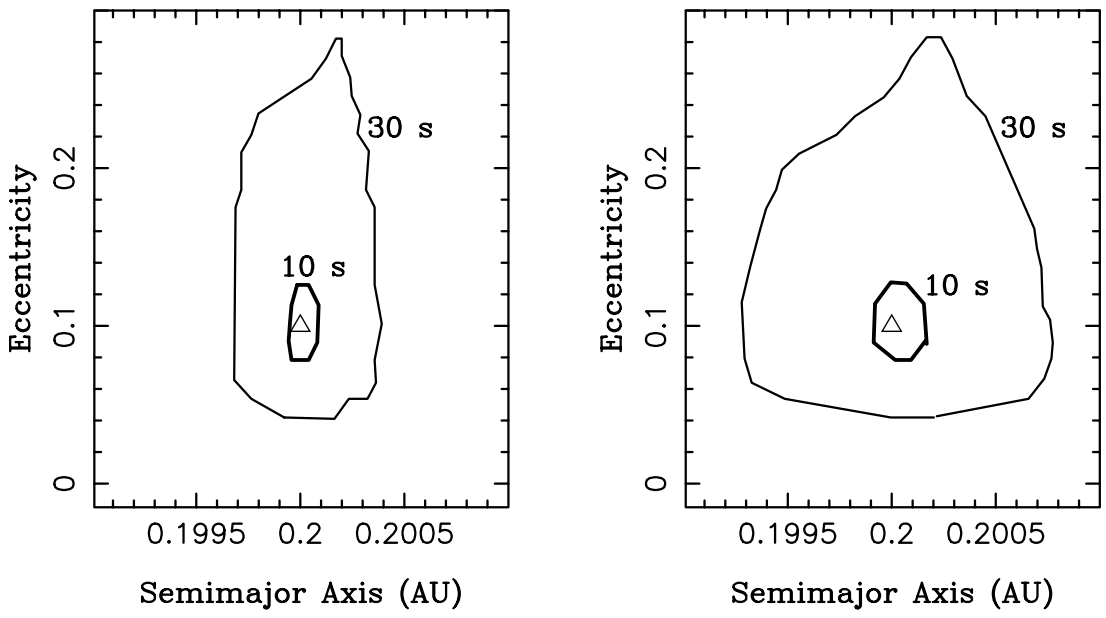

FIG. 11.— Same as Fig. 9, but for 43 (*left*) and 22 transits (*right*). This figure demonstrated the increased uncertainty in the determined parameters when small number of transits are available.

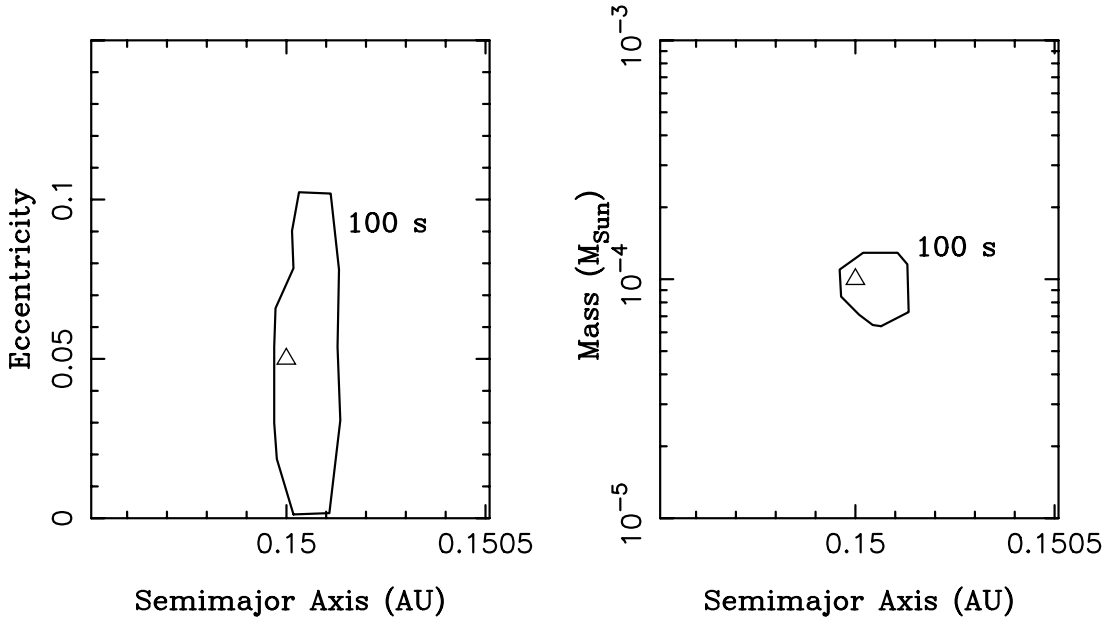

FIG. 12.—Same as Fig. 9, but for our case-3 planetary system (see Fig. 3). The parameters of the perturbing planet, denoted by a triangle in each panel, are $m_2 = 10^{-4} m_0$, $a_2 = 0.15$ AU, and $e_2 = 0.05$. The contour line shows the envelope of solutions with $\eta_{\rm cut} = 100$ s.

realistic values of $\eta_{\rm cut}$, because the filtered short-period signal has only a small amplitude. Specifically, we find that with $\eta_{\rm cut} = 5$ s the best-fit solution are $2\times10^{-5} < m_2/m_0 < 1.2\times10^{-4}$, $0.2485 < a_2 < 0.2505$ AU, and $e < 0.25$. Already for $\eta_{\rm cut} > 5$ s, however, the PT method is unable to uniquely identify a_2 and picks up a range of incorrect solutions. Therefore, the precision of the TTV measurements better than $\sim$5 s would be probably required in this example. (We stress that these issues do not stem from the inaccuracy of the PT method discussed in § 3. Low S/N of the TTV measurements could prevent characterization of the perturbing planet regardless the method used for fitting.)

Finally, we used equation (23) and the appropriate cuts on $\Delta\chi^2$ to calculate the confidence regions of parameters m_2, a_2, and e_2 for different values of $\sigma_{\rm wn}$. In general, we found that the correct solution can be identified at high confidence levels ($\gtrsim$99%) for values of $\sigma_{\rm wn}$ that are at least somewhat smaller than the uniqueness thresholds of $\eta_{\rm cut}$ established above. For $\sigma_{\rm wn}$ exceeding these thresholds, namely $\sigma_{\rm wn} > 15$, 10, 100, and 5 s for cases 1, 2, 3, and 4, respectively, the perturbing planet would be difficult to characterize from TTVs alone.

4.2. *Five-parameter Fits*

The results obtained with the five-parameter fits, where we allowed $\lambda_2^{(0)}$ and $\varpi_2^{(0)}$ to vary (in addition to m_2, a_2, and e_2), show little difference with respect to those obtained with the three-parameter fits. In general, the region of acceptable fits with $\eta < \eta_{\rm cut}$ becomes about a factor of $\sim$2 wider in a_2 than that obtained previously (Figs. 9, 11, and 12). This is due to the fact that a slight change in a_2 may be compensated by modifying the values of $\lambda_2^{(0)}$ and $\varpi_2^{(0)}$ so that the resulting η value remains roughly unchanged. This mainly affects fits to the TTVs with a short time baseline. Interestingly, we find that the range of the estimated m_2 and e_2 values obtained from the five-parameter fit is similar to that obtained for the three-parameter fit (independently of the length of the TTV time baseline). Therefore, the discussion in § 4.1 of the white noise effects on the results is also valid here.

We found that the values of $\lambda_2^{(0)}$ and $\varpi_2^{(0)}$ can be correctly constrained from the data (Fig. 13), although the uncertainty can

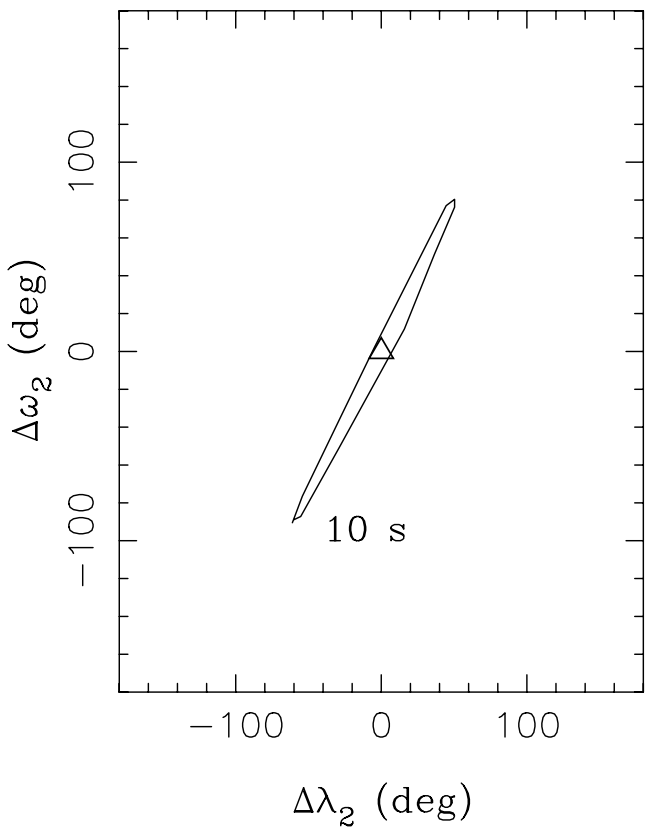

FIG. 13.—Range of acceptable values obtained for our case-1 planetary system (see Fig. 3) with the five-parameter fit. We plot $\Delta\lambda_2 = \lambda_{2,\rm est} - \lambda_2^{(0)}$ and $\Delta\varpi_2 = \varpi_{2,\rm est} - \varpi_2^{(0)}$, where $\lambda_{2,\rm est}$ and $\varpi_{2,\rm est}$ are the estimated values from the five-parameter fit, and $\lambda_2^{(0)}$ and $\varpi_2^{(0)}$ are the original values that we used to set up the test. The triangle denotes the best-fit solution. The contour line shows the envelope of solutions with $\eta_{\rm cut} = 10$ s.

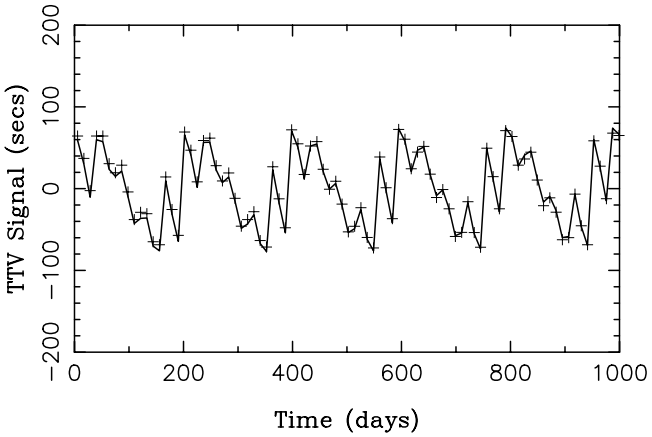

FIG. 14.—Same as Fig. 1, but for the secondary transits. The solid line shows the transit times for the best-fit solution ($m_2 = 0.97 \times 10^{-4} m_0$, $a_2 = 0.2$ AU, and $e_2 = 0.102$) that we obtained with the PT method from 87 primary and 87 secondary consecutive transits. Plus signs show the secondary transit times for the original parameters ($m_2 = 10^{-4} m_0$, $a_2 = 0.2$ AU, and $e_2 = 0.1$).

be large. For example, the best-fit values for the case 1 fall dead on the $\lambda_2^{(0)}$ and $\varpi_2^{(0)}$ values that we used to set up the test. With $\eta_{\rm cut} = 10$ s, however, the estimated values of $\lambda_2^{(0)}$ and $\varpi_2^{(0)}$ are spread over a wide range ($\approx 80^\circ$) about the correct solution. There also appears to be strong correlation between the estimated values of $\lambda_2^{(0)}$ and $\varpi_2^{(0)}$ with larger values of $\lambda_2^{(0)}$ corresponding to larger values of $\varpi_2^{(0)}$ (Fig. 13). Similar correlations were found for all tested planetary systems.

4.3. *Secondary Transits*

The timing of secondary transits (when the planet passes beyond the star) can also help to detect and characterize the unseen planet in the system. As discussed in Heyl & Gladman (2007), the secondary transits can be especially useful to detect the long-term effects such as the apsidal precession produced by the perturbing planet. Here we concentrate on the effects of the *short-period* variations in the timing of secondary transits.

As in §§ 4.1 and 4.2, we performed tests with $m_0 = M_{\rm Sun}$, $a_1 = 0.1$ AU, $e_1 = 0$, and $T_{\rm int} = 1000$ days (producing 87 primary and 87 secondary transits). Unlike in §§ 4.1 and 4.2, however, we then used *both* the primary and secondary transits to estimate the parameters of the perturbing planet from the PT method. Given the results obtained in § 4.2, which demonstrate that the three- and five-parameter fits are similar, we used the three-parameter method here to economize the CPU time. Below we discuss the results obtained for the four representative cases shown in Figs. 1–3 and 6*b*.

The envelope of acceptable solutions with $\eta < \eta_{\rm cut} = 10$ and 30 s for case 1 is very similar to that shown in Figure 9, where we did not use secondary transits. Figure 14 illustrates our best fit to the 87 secondary transit times (the fit to the 87 primary transit times is very similar to the solid line shown in Fig. 1). When fewer transits are used, we identify trends very similar to those already described in § 4.2 and illustrated in Figure 11. Specifically, the envelope of solutions becomes wider in a_2 and remains about the same in m_2 and e_2. The results for cases 2, 3, and 4 show the same behavior. Therefore, we conclude that (1) the secondary transits do not help much to improve the precision of results, and (2) the correct solution can be identified with a relatively small number ($\sim$20) of (primary and/or secondary) transits.

The secondary transits can be very important to ensure the uniqueness of the results. As we discussed in § 4.2, the unique solution in case 1 was achieved from primary transits alone with $\eta_{\rm cut} < 15$ s, assuming that at least $\sim$20 primary transits were observed. If, in addition to $\sim$20 primary transits, at least $\sim$20 secondary transits were also observed, the uniqueness is ensured for $\eta_{\rm cut} < 25$ s, thus placing a weaker requirement on the precision of the timing measurements (here we assume that the timing of primary and secondary transits is measured with equal precision). We found a similar increase in the critical η value (by $\sim$50%–100%) in cases 2, 3, and 4. Therefore, observations of secondary transits can be very important to achieve an unique determination of the perturbing planet parameters from the TTVs.

4.4. *Gaps in Transit Observations*

Above we assumed that observations of the *consecutive* transit times are available. This is generally not the case of real observations where long delays may occur between different sets of telescopic observations and/or transits may be observed with a diluted sampling. We tested such effects by introducing artificial gaps in our synthetic TTV series, by sampling every second, third, or fourth consecutive transit, etc. We found that the total number of observed transits, rather than their time distribution, determines whether or not a unique and correct solution can be identified from the short-period timing variations of transits. A longer time base of transit observations can be important to characterize the resonant and long-period components in the TTV signal.

5. CONCLUSIONS

Above we discussed our attempts to determine the parameters of the perturbing planet by the least-squares fit to the TTV signal. We found that the PT method can sample the parameter space about 10^4 times faster than the *N*-body integrations. The white noise threshold that allows for unique and correct solutions of the inverse problem varies from case to case but is typically a small fraction ($\sim$15%–30%) of the full TTV amplitude. Therefore, while the planet detection can be achieved from TTVs with relatively large $\sigma_{\rm wn}$ values, the determination of the planet's parameters is a more delicate problem and may require very high precision measurements.

What is the optimal observing strategy to characterize a planetary system from the TTVs? Based on the tests described in § 4, we observe that (1) the high-precision measurements of at least $\sim$20 transits (primary or secondary) are generally needed to ensure the uniqueness of the results; (2) if $\gtrsim$20 transits were observed, it may be beneficial to dilute the sampling and look for the long-term trends in the timing of (ideally both) the primary and secondary transits such as the ones produced by the resonant and long-period effects; (3) observations of secondary transits can be very useful to achieve the uniqueness as they help to increase the sampling frequency of the diagnostic short-period variations in the signal; (4) the total number of the observed transits (rather than their time distribution) is central to the inversion process; and (5) the very high precision measurements will be needed to characterize a planetary system with small perturbing planets.

The PT method discussed in this paper can be generalized to account for (1) eccentric orbit of the transiting planet, and (2) planetary systems with inclined orbits. Improved precision near the mean motion resonances can be achieved by using a higher-order perturbation theory. The problem with the divergence of the Laplacian expansion for high eccentricities can be resolved by using the Beaugé's expansion (Beaugé 1996) of the disturbing function, which is valid even for crossing planetary orbits. Moreover, efficient minimum-seeking methods (such as

the genetic algorithm, "simulated annealing" method, etc.; e.g., Beaugé et al. 2008) can be implemented in the algorithm to search for the best-fit solutions rather than using a simple grid technique used here. These developments are left for future work.

This work was supported by the National Science Foundation. We thank Dimitri Veras, who helped us with Figure 5. We also thank David Charbonneau, Daniel Fabrycky, Darin Ragozzine, and Jeremy Heyl for their comments on this work.

REFERENCES

Agol, E., & Steffen, J. H. 2007, MNRAS, 374, 941
Agol, E., Steffen, J., Sari, R., & Clarkson, W. 2005, MNRAS, 359, 567
Beaugé, C. 1996, Celest. Mech. Dyn. Astron., 64, 313
Beaugé, C., Giuppone, C. A., Ferraz-Mello, S., & Michtchenko, T. A. 2008, MNRAS, 385, 2151
Brouwer, D., & Clemence, G. M. 1961, Methods of Celestial Mechanics (New York: Academic Press)
Deprit, A. 1969, Celest. Mech., 1, 12
Ellis, K. M., & Murray, C. D. 2000, Icarus, 147, 129
Gladman, B. 1993, Icarus, 106, 247
Heyl, J. S., & Gladman, B. J. 2007, MNRAS, 377, 1511
Holman, M. J., & Murray, N. W. 2005, Science, 307, 1288
Hori, G. 1966, PASJ, 18, 287
Kaula, W. M. 1962, AJ, 67, 300
Morbidelli, A. 2002, Modern Celestial Mechanics: Aspects of Solar System Dynamics (London: Taylor & Francis)
Press, W. H., Teukolsky, S. A., Vetterling, W. T., & Flannery, B. P. 1992, Numerical Recipes in FORTRAN: The Art of Scientific Computing (Cambridge: Cambridge Univ. Press)
Šidlichovský, M. 1990, Bull. Astron. Inst. Czech. Acad. Sci., 42, 116
Steffen, J. H., & Agol, E. 2005, MNRAS, 364, L96
Sundman, K. F. 1916, Öfversigt Finska Vetenskaps-Soc. Förh., 58 A, 24
Torres, G., Winn, J. N., & Holman, M. J. 2008, ApJ, 677, 1324